Journal of Applied Polymer Science

Generation of nanofibers via electrostatic-induction-assisted solution blow spinning

Dingyou Tang, Xupin Zhuang, Chan Zhang, Bowen Cheng, Xiaojie Li
College of Textiles, Tianjin Polytechnic University, Tianjin 300387, People's Republic of China
Correspondence to: X. Zhuang (E-mail: zhxupin@tjpu.edu.cn)

ABSTRACT: Increasing attention has been given to nanofiber fabrication techniques. Solution blow spinning (SBS) is an innovative, simple, and effective method for producing nanofibers, and it only uses the drawing force of high-velocity airflow. However, solution-blown nanofibers easily form bundles; this results in an uneven distribution of nanofibers and an inhomogeneity of nanofiber mats. In this study, electrostatic-induction-assisted solution blow spinning (EISBS) was established by the introduction of an additional electrostatic field with an induction circle electrode into the SBS system. The effects of the electrostatic force on the fiber configuration and structure were examined. The results indicate that the electrostatic field effectively separated the fibers. Response surface methodology, based on the four-factor, three-level Box–Behnken design, was used to facilitate a more systematic understanding of the processing parameters of EISBS. © 2015 Wiley Periodicals, Inc. J. Appl. Polym. Sci. **2015**, *132*, 42326.

KEYWORDS: electrospinning; fibers; manufacturing; microscopy; porous materials

Received 21 September 2014; accepted 7 April 2015
DOI: 10.1002/app.42326

INTRODUCTION

As an important one-dimensional nanomaterial, nanofibers have an extremely high specific surface area and are highly porous with excellent pore interconnectivity.[1] These unique characteristics and functionalities have imparted nanofibers with tremendous potential applications, such as in biomedical engineering,[2] wound healing,[3] drug delivery and release control,[4,5] composite reinforcement,[6] energy harvest and storage,[7] and many others. As a result, nanofiber manufacturing techniques have attracted much attention in academic and industrial fields in recent years.[8] A variety of synthetic methods have been developed for preparing polymer or polymer/metal precursor nanofibers; these include self-assembly,[9] interfacial polymerization,[10] seeding growth,[11] oligomer-assisted polymerization,[12] electrospinning,[13] centrifugal spinning,[14] and solution blow spinning (SBS).[15,16]

Among the methods mentioned, SBS is a process that spins nanofibers from polymer solutions and only uses high-velocity gas flow as the driving force for fiber formation.[17,18] This method increases the yields and reduces the costs of manufacturing nanofibers.[19] Previous reports have indicated the use of several synthetic and natural polymers, including poly(methyl methacrylate),[20] polystyrene,[21] poly(lactic acid),[22] polyacrylonitrile (PAN), and cellulose, to successfully spin nanofibers. Sinha-Ray *et al.*[23] introduced a novel process of solution coblowing to core–shell poly(methyl methacrylate)–PAN fibers and a posttreatment technique that resulted in mesoscopic carbon tubes. Meanwhile, Zhuang *et al.*[24] successfully used a multiorifice die on solution-blown poly(vinylidene fluoride) to form nanofibrous mats. These studies demonstrated that SBS is a simple and effective method for the production of polymer nanofibers and is expected to be developed as an important method for mass production.[24]

However, solution-blown nanofibers easily form bundles because of the influence of airflow.[25] These bundles result in an uneven distribution of the nanofibers and inhomogeneity of nanofiber mats; thereby, this yields poor performances in several fields (e.g., filtration, composite reinforcement).[26] Thus, finding a way to separate fibers from bundles is necessary. An electrostatic field is an effective means of separating charged or polarized particles and fibers.[27] Electrostatic separation has been successfully applied to separate spunbond fiber bundles into individual fibers.[28] Electrostatic fields are also used in electrostatic sprays to improve atomization.[29] Electrospinning, which was developed from electrostatic sprays, is a process in which submicrofibers are produced with an electrostatically driven jet of a polymer solution.[30] This method proves that the electrostatic force is a drag force in solution jet stretching. Compared to electrospinning, the SBS process can produce fibers with different morphologies and crystallization properties; this results in different application performances.[30]

Among the ways of applying voltage, induction-charging is often used to apply potential because high voltages do not

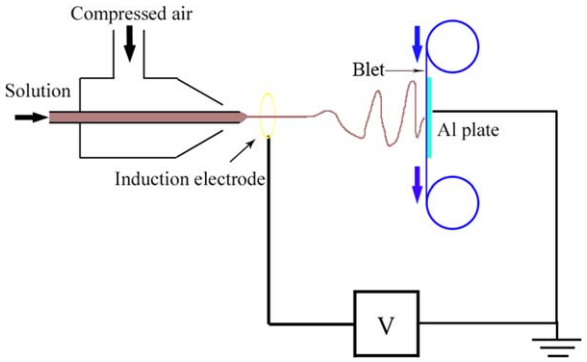

Figure 1. Schematic of the electrostatic-induction-assisted solution blow apparatus. [Color figure can be viewed in the online issue, which is available at wileyonlinelibrary.com.]

directly come in contact with spray liquids. This method requires a low voltage and operating current. The low voltage requirement also makes the operating conditions safer.[31] To overcome the shortcomings of uneven fiber distribution in nanofiber mats, we implemented an electrostatic induction to apply electrostatic features to the conventional solution-blowing system. We termed this new technique *electrostatic-induction-assisted solution blow spinning* (EISBS).

To optimize the parameters of EISBS, response surface methodology (RSM) was adopted.[32] RSM is a collection of statistical and mathematical techniques that are beneficial for developing, improving, and optimizing processes. This method allows synchronous statistical investigation of single-factor and interactive effects. It also reduces the number of experimental runs needed for statistically acceptable results compared with full-factorial experiments.[33] In this work, RSM was performed to investigate the effect of variation of the process parameters that control fiber formation.

EXPERIMENTAL

Description of the Setup and Experimental Procedure

Figure 1 illustrates the setup for EISBS, which was a modification of our previous SBS apparatus.[34] A circular copper induction electrode (diameter = 20 mm) was located 5 mm below the spinning nozzle. Subsequently, a grounded aluminum metal plate was placed under a polyporous belt (no gap between the Al plate and belt). Induction voltage (0 kV–50 kV) was applied on the circular electrode to form an electrostatic field. EISBS spinning is briefly described as follows: the polymer solution stream was pressed out by an injection pump from the nozzle and was then extremely drawn by the high-speed airflow from the coaxial outlet and electrostatic force. Nanofibers were formed and deposited on the belt (collection distance = 20–100 cm, belt speed = 0–5 cm/s) by the evaporation of the solvents.

Preparation of the Polymer Solutions

PAN (average molecular weight ≈ 100,000) powder and *N,N*-dimethylformamide (99%) were purchased from Sigma-Aldrich Chemical Co. (Shanghai, China). PAN solutions with 8, 10, 12, and 14 wt % concentrations were prepared by the dissolution of PAN powder in *N,N*-dimethylformamide and then stirred for 12 h until complete dissolution occurred at room temperature.

Table I. Independent Variables and Their Levels in the Experimental BBD

Factor	Code	−1	0	+1
Voltage (kV)	A	5	15	25
Air pressure (MPa)	B	0.1	0.15	0.2
Feed rate (mL/h)	C	5	10	15
Collection distance (cm)	D	20	40	60

Preparation of the Nanofiber Mats with Different Levels of Voltage Induction

To examine the effect of induction of voltage on the fiber morphology, we produced a nanofiber mat with four levels of induction voltage (0, 10, 20, and 25 kV). The other parameters for EISBS were 12 wt % (solution concentration), 0.15 MPa (air pressure), 20 mL/h (solution feed rate), and 40 cm (collection distance). Each sample was spun for 10 min. The collected nanofibers mats were initially dried *in vacuo* at room temperature for 24 h before further investigation.

Systematic Study of the Effects of Four Parameters on the Fiber Diameter

A standard RSM design, called the *Box–Behnken design* (BBD), was performed to investigate and identify the relationship between the fiber diameter and the processing variables.[35] This type of design defines the minimum number of experimental combinations in the experimental domain to be explored to obtain the maximum information for adjusting the proposed model. For a quadratic model, experiments must be performed for at least three levels of each factor.[35] Each of these levels are best chosen and equally spaced. The four independent variables were voltage (*A*), air pressure (*B*), feed rate (*C*), and collection distance (*D*). We coded at three levels: −1, 0, and +1. The factors and their corresponding levels (coded and actual) chosen in the four-factor, three-level BBD are shown in Table I. The average diameter of the fibers observed from each experiment was used as the response value. The ranges of the variables were selected from preliminary one-factor-at-a-time experiments, wherein the nanofibers were confirmed to be produced in the EISBS process. There were 29 experiments in random running order. The design points and experimental data are shown in Table II.

Morphological Studies of the Nanofiber Mats Spun by EISBS

The morphology of the PAN nanofibers was observed via field emission scanning electron microscopy (SEM; Hitachi S-4800, imaging voltage = 10 kV) after being gold-coated with a sputter coater. We determined the average diameters of the nanofibers from about 100 random measurements by analyzing the micrographs of their morphologies with image processing software (Image-Pro Plus).

RESULTS AND DISCUSSION

Effect of the Solution Concentration on the Fiber Morphology

In solution blowing, the solution viscosity has an important function in determining the range of concentrations from which

Table II. Experiments in the Randomizing Running Order

Experiment number	A	B	C	D
1	25	0.2	10	40
2	25	0.15	10	20
3	5	0.15	5	40
4	5	0.15	15	40
5	25	0.15	15	40
6	15	0.2	5	40
7	5	0.15	10	20
8	15	0.15	5	60
9	15	0.15	5	20
10	15	0.15	15	60
11	15	0.2	15	40
12	15	0.2	10	60
13	15	0.1	5	40
14	15	0.15	10	40
15	25	0.15	5	40
16	5	0.1	10	40
17	5	0.15	10	60
18	15	0.15	10	40
19	25	0.15	10	60
20	15	0.2	10	20
21	15	0.15	10	40
22	15	0.1	10	20
23	15	0.1	15	40
24	25	0.1	10	40
25	15	0.1	10	60
26	15	0.15	15	20
27	5	0.2	10	40
28	15	0.15	10	40
29	15	0.15	10	40

continuous fibers can be obtained.[36] A continuous fibrous structure was obtained above a critical solution concentration, and the fiber morphology was also affected by the solution concentration. When the concentration of the solution was optimized with the process parameters, continuous nanofibers were produced. To ensure that the concentration matched, solutions with four levels of concentration were prepared and spun via the EISBS process with practicable parameters (0.15 MPa, 15 kV, 15 mL/h, and 40 cm). The SEM photographs of fibers spun from solutions with 8, 10, 12, and 14 wt % concentrations are illustrated in Figure 2.

As shown in Figure 2(a), small nanofibers were successfully synthesized when the solution concentration was 8 wt %. However, dense beads were also obtained. The formation of continuous fiber were attributed to extensive chain entanglements in the polymer solution. At a high solvent concentration, there is a greater tendency for solvent molecules to segregate polymer molecules from entanglement during spinning.[37] Smooth fiber morphology were observed starting from a solution concentration of 10 wt %. The fibers were thicker, and a percentage of the beads merged into the fibers [Figure 2(b)]. This was attributed to the higher viscosity of solutions, and this resulted in a lower surface tension and eventually decreased the formation of beads.[37] Moreover, a high concentration of solutions reduced the effect of solvent molecule segregation. In Figure 2(c), a net of interconnected and continuous fibers was formed, and no beads were found on the fibers for the case of 12 wt % concentration. However, when the concentration was increased to 14 wt %, the fibers became thicker than those presented in Figure 2(c). The fiber diameter increased with the solution concentration. Smaller diameters obtained at lower concentrations were related to the higher mobility of the polymer chains in the jet during the spinning process.[38] As shown in Figure 2, 12 wt % was the optimal solution concentration for EISBS.

Effect of Electrostatic Induction on Nanofiber Separation

Electrospinning is a process to known fabricate nanofibers with high-power electrostatic force.[39] Moreover, several studies have introduced gas flow into the electrospinning system to overcome the high surface tension of the polymer solution and to produce nanofibers from polymers that are difficult to spin [e.g., hyaluronic acid (HA)].[39–41] In EISBS, an additional electrostatic field was introduced into SBS in a different way to enhance the fabrication of nanofibers with dispersive properties.

To investigate the effect of electrostatic induction on the fiber morphology, a series of experiments were performed with a 12 wt % PAN/*N*,*N*-dimethylformamide solution, which was selected from the previous experiments. Figure 3 shows the fabricated nanofibers via EISBS with different induction voltages. Figure 3(a) illustrates that a mass of fibers that were stuck together and rolled into bundles; the nanofiber did not disperse well without an applied electrostatic induction force. When a 10-kV induction voltage was applied, a homogeneous nanofiber distribution with few bundles was produced [Figure 3(b)]. As shown in Figure 3(c), under the effect of a 20-kV induction voltage, the fiber bundles rarely appeared. However, the fibers were still stuck to one another in the overlying cross point. Moreover, as shown in Figure 3(d), the fibers were well separated, and no fiber bundle was found when a 25-kV induction voltage was applied. The distribution of the nanofibers became highly homogeneous with increasing voltage, and the characteristics of the single filaments were more noticeable for voltages higher than 20 kV. The results indicate that electrostatic fields aided in separating fiber bundles into single fibers and promoted nanofiber dispersive properties. At different conditions of induction voltages, the diameters of the nanofibers also showed a significant difference.

Statistical Analysis of RSM

The BBD model was chosen to perform a series of experiments to fully characterize the parameters of EISBS. In addition, an analysis of variance for the experimental response was carried out to evaluate the quadratic approximation of the BBD response surface model (Table III). The statistical significance of the data was assessed on the basis of the p value (listed in Table III), wherein the factor had a significant effect on the response when the p value was less than 0.05, whereas the factor had no significant impact on the response when the p value was greater

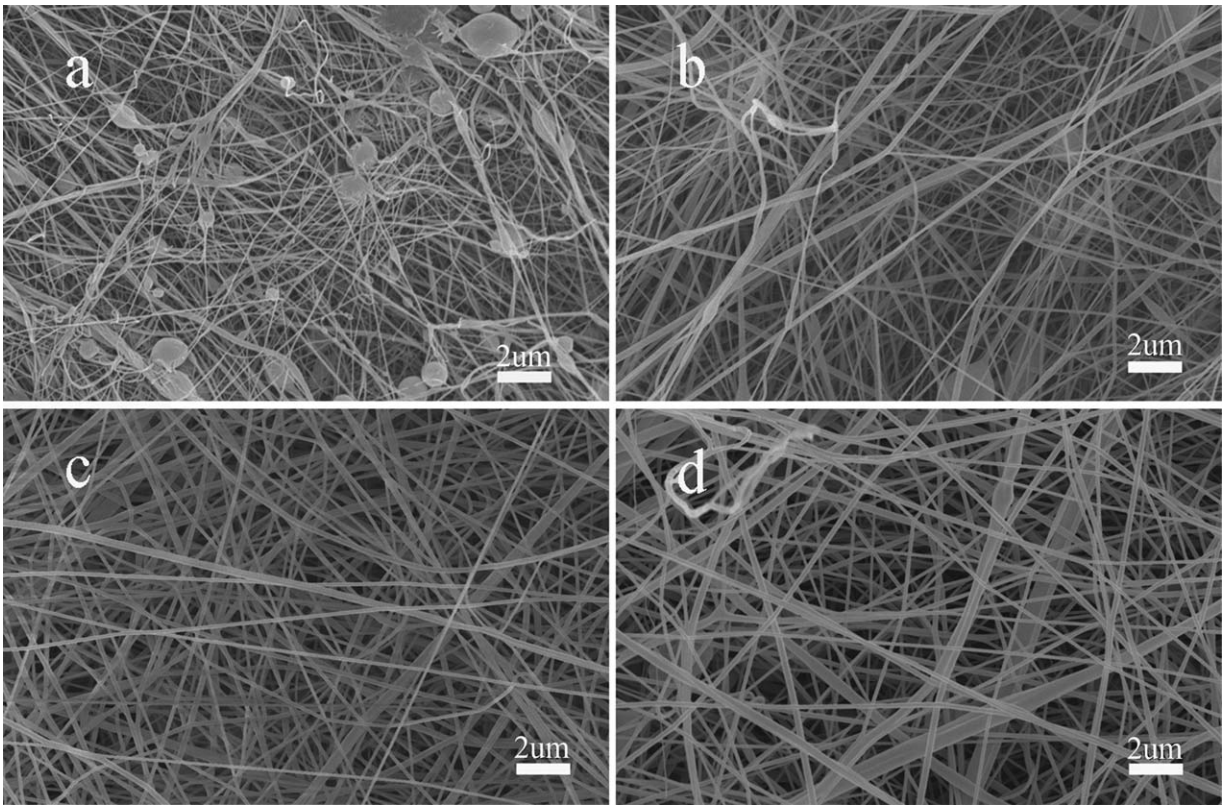

Figure 2. SEM photographs of fibers spun from solutions with concentrations of (a) 8, (b) 10, (c) 12, and (d) 14 wt %.

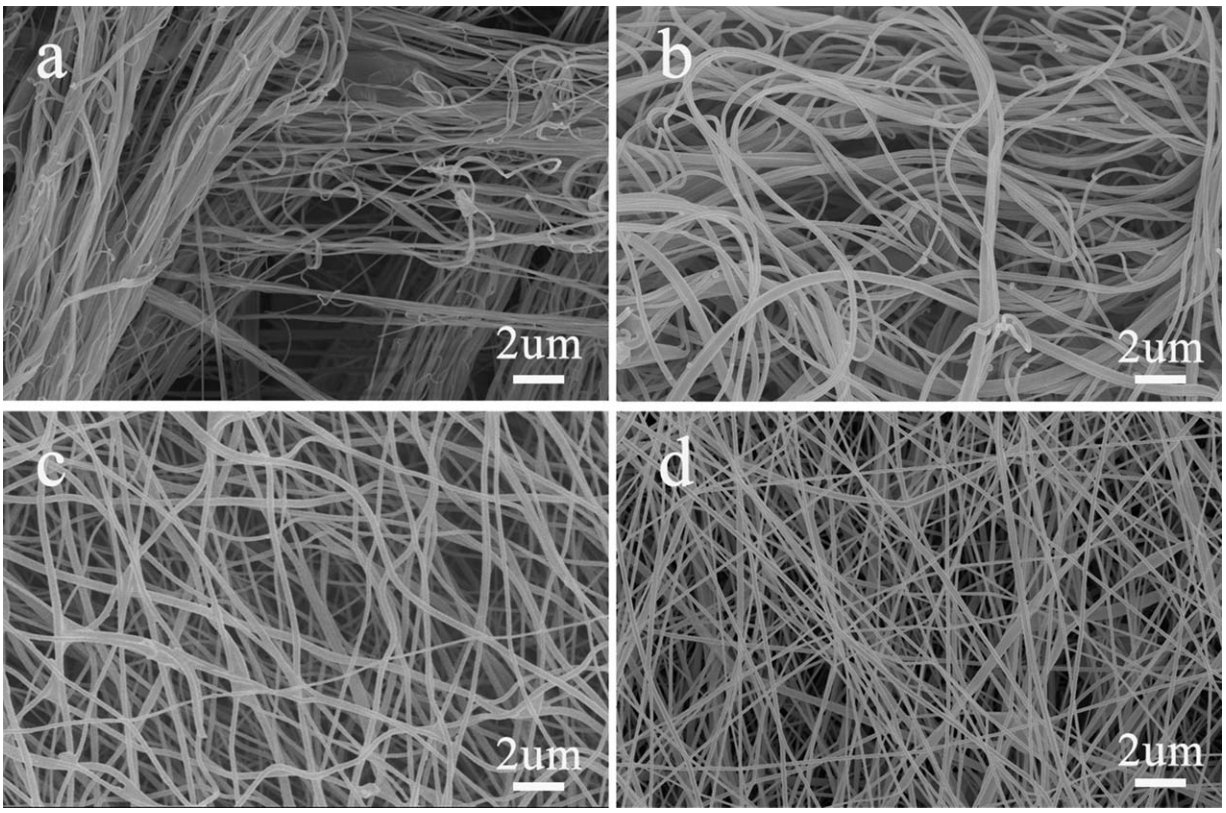

Figure 3. SEM micrographs of the nanofibers with voltages of (a) 0, (b) 10, (c) 20, and (d) 25 kV.

Table III. Analysis of Variance for the Response Surface Model

	Sum of squares	Degrees of freedom	Mean square	*F* value	*p* value[a]
Model	9115	14	651.07	4.48	0.0041
A	1803.86	1	1803.86	12.4	0.0034
B	1164.57	1	1164.57	8.01	0.0134
C	438.64	1	438.64	3.02	0.1044
D	236.34	1	236.34	1.63	0.2231
AB	193.84	1	193.84	1.33	0.2676
AC	1400.86	1	1400.86	9.63	0.0078
AD	870.78	1	870.78	5.99	0.0282
BC	23.82	1	23.82	0.16	0.6918
BD	79.96	1	79.96	0.55	0.4707
CD	390.08	1	390.08	2.68	0.1237
A^2	16.66	1	16.66	0.11	0.74
B^2	1633.04	1	1633.04	11.23	0.0048
C^2	678.46	1	678.46	4.67	0.0486
D^2	634	1	634	4.36	0.0556

[a] Statement describing *F*.

than 0.05.[42] A model *F* value of 4.48 implied that the model was significant and available. A, B, AC, AD, B^2, and C^2 had a significant impact on the average diameters of the nanofibers. The R^2 value represents the proportion of the total variability that has been explained by the regression model. An R^2 value near 1 is desirable.[42] On the other hand, the lack-of-fit value compares the residual error from the model error to the pure error from replicated experiments. A significant lack of fit means that the polynomial model does not fit well with all of the design points.[42] For this experiment, an R^2 value of 0.9174 and a lack-of-fit value of 1.94 implied that the model used for predicting the response based on the parameters considered was valid enough.

The observed fiber diameters were compared with the predicted values [Figure 4(a)], and a linear correlation coefficient was calculated. The result show that the predicted values were in line with the actual experimental outcome. Furthermore, a linear correlation coefficient of 0.9473 also indicated a valid correlation between the experimental data and the theoretically predicted values within the design space. The probability plot of the studentized residuals was demonstrated [Figure 4(b)] to check off the normality assumption. The plot indicated the normality in the error term because the residuals were approximately linear. The normal probability distribution of residuals confirmed that the variation of the model predicted values from the experimental consequences was random (no systematic bias).

Optimization Studies of Process Parameters in EISBS

The average diameter of the fibers observed from each experiment was used as the response value. The three-dimensional

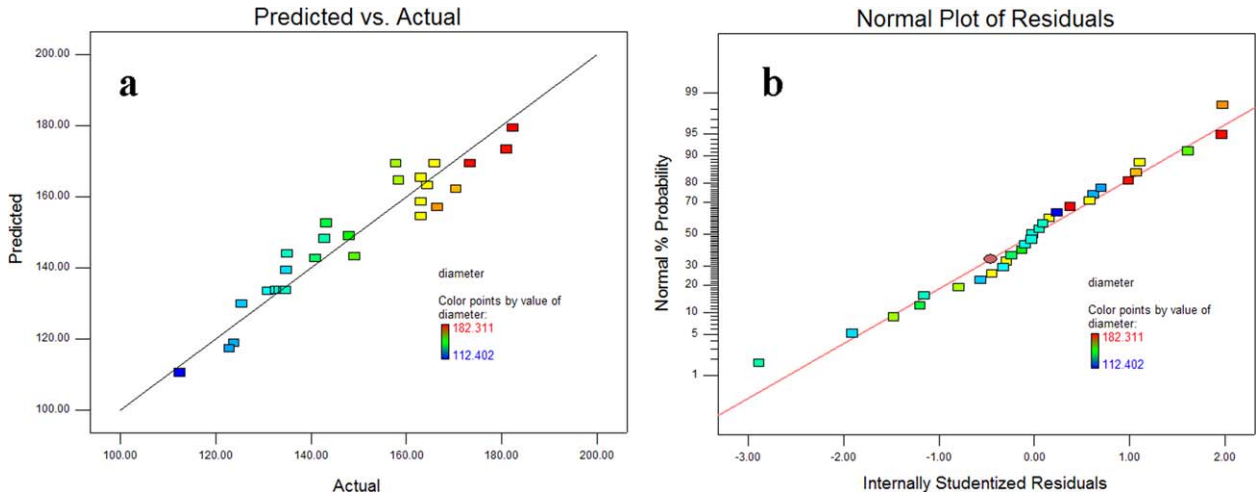

Figure 4. Assessment of the accuracy of the response surface model: (a) plot of the model-predicted fiber diameters versus the experimental values and (b) normal probability plot of the studentized residuals. [Color figure can be viewed in the online issue, which is available at wileyonlinelibrary.com.]

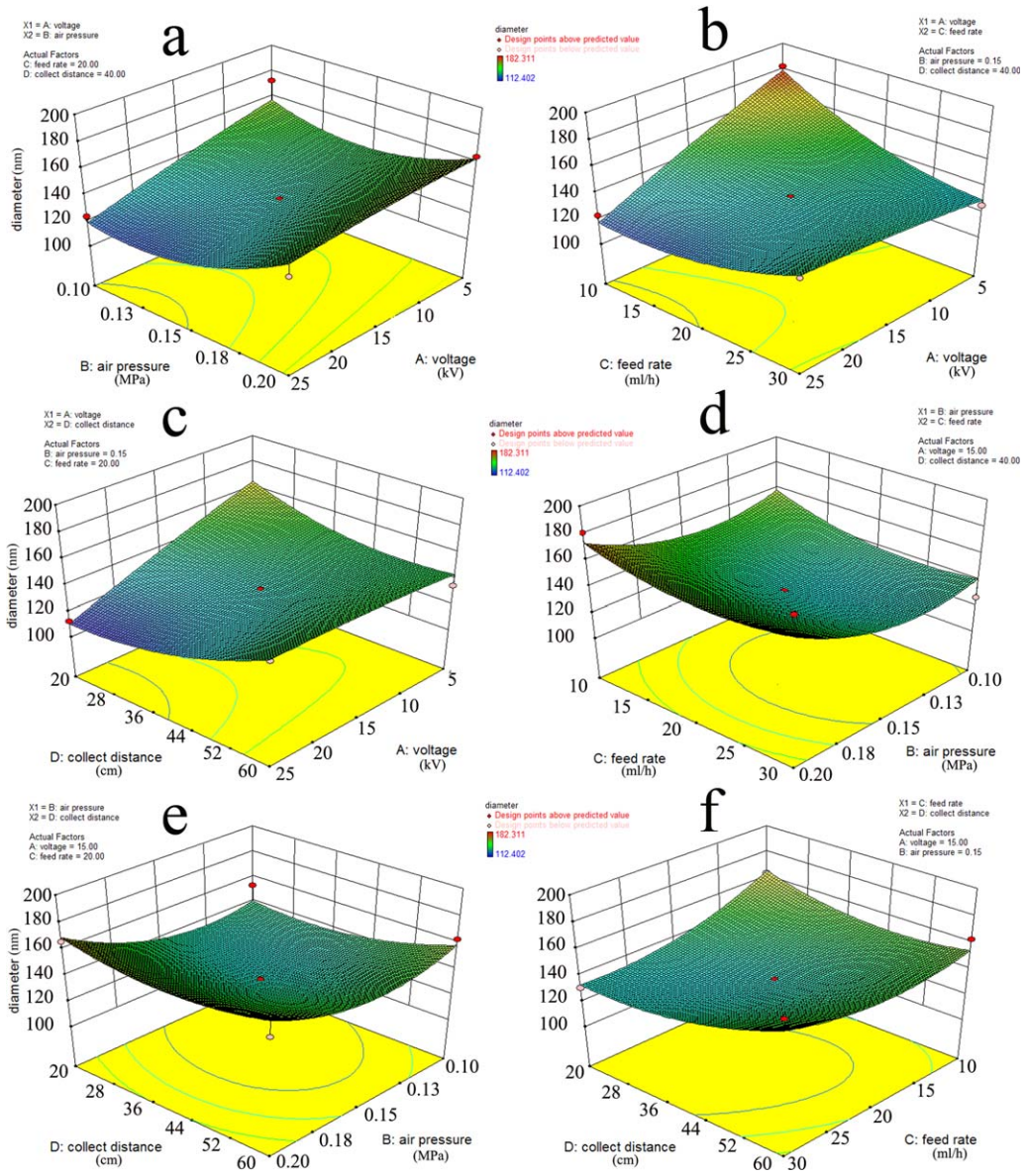

Figure 5. 3D surface plots of the average fiber diameters for various parameters. [Color figure can be viewed in the online issue, which is available at wileyonlinelibrary.com.]

(3D) surface plots of the response variable (average diameters of the nanofibers) as a function of the selected factors (two-factors-at-a-time) are illustrated in Figure 5(a–f). We shaped the 3D surface plots, showing the graphical display of the fitted regression model, by combining the points of identical response values (identical fiber diameters).

Effect of the Induction Voltage on the Fiber Morphology. The response surfaces of the average diameters of the nanofibers, in nanometers, as a function of the applied voltage are shown in Figure 5(a–c). As shown in Figure 5(a), the increase in the induction voltage from 5 to 25 kV decreased the fiber diameter from 158 to 117 nm when the air pressure was fixed at 0.1 MPa. At a low feed rate (10 mL/h), the fiber diameter decreased from 180 to 120 nm when the induction voltage was increased from 5 to 25 kV [Figure 5(b)]. Moreover, at a low collection distance (20 cm), the fiber diameter also decreased from 165 to 110 nm when the induction voltage was increased from 5 to 25 kV. The three figures indicate that the resulting fiber diameter was very responsive to the changes in voltage, as expected. The average diameters of nanofibers were low after the applied induction voltage was increased from 5 to 25 kV while the other three factors remained fixed. The impact of the electrostatic force on the average diameters of the nanofibers was similar to the investigated effect of the voltage on electrospinning. Generally, a higher voltage leads to a stronger electrostatic force, and this results in a decrease in the surface tension and a greater splitability of the solution jet.[43] Therefore, the average diameter of manufactured fibers decreased with a sustained increase in voltage.

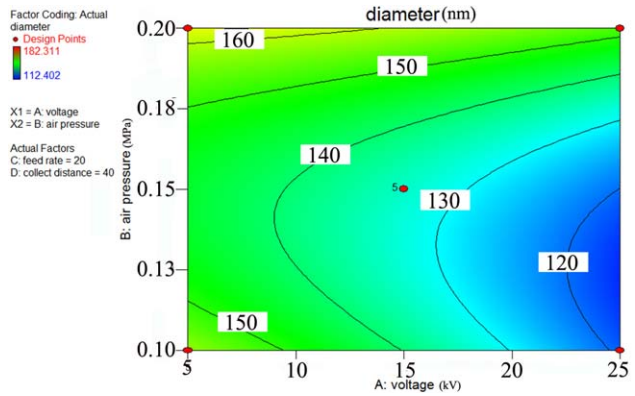

Figure 6. Two-dimensional surface plots of the average fiber diameters for the voltages and air pressures. [Color figure can be viewed in the online issue, which is available at wileyonlinelibrary.com.]

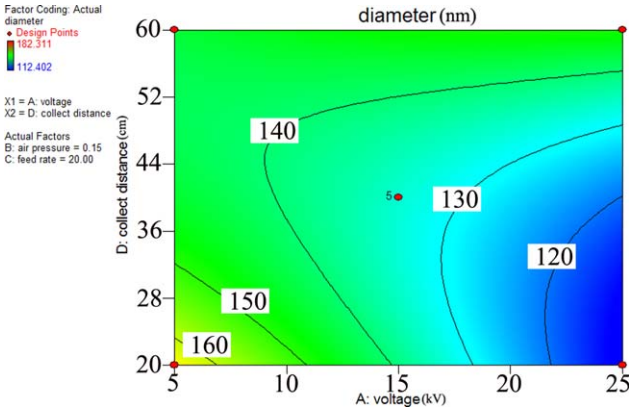

Figure 7. Two-dimensional surface plots of the average fiber diameters for the collection distances and induction voltages. [Color figure can be viewed in the online issue, which is available at wileyonlinelibrary.com.]

Effect of the Air Pressure on the Fiber Morphology. The response surfaces of the average diameters of the nanofibers, in nanometers, as a function of the air pressure are illustrated in Figure 5(a,d,e). The impact of the air pressure was constrained by the applied voltage to a particular extent (also shown in Figure 6). The average diameters of the nanofibers decreased from 153 to 143 nm and then increased to 162 nm with increasing air pressure from 0.1 to 0.2 MPa for an applied voltage of 5 kV. In our previous research, we observed that the addition of air pressure initially reduced the fiber diameter, which was then slightly enhanced with SBS.[24] However, at a high voltage such as 25 kV, the average diameters of the nanofibers increased when the air pressure was increased from 0.1 to 0.2 MPa. When the air pressure was 0.2 MPa, the average diameter of the nanofibers was close to 160 nm, and when the air pressure was 0.1 MPa, the average diameter of the nanofibers was slightly larger than 120 nm. At a higher voltage, the drag force, including the air shear force and electrostatic force, applied on the solution jet had a greater effect on the fiber diameter. This observation revealed that the exorbitant drag force, including the air pressure and electrostatic force, reduced the flight time of the solution jets and evaporated the solution too fast; this finally enhanced the fiber diameter. The result shows that the air pressure had a strong interactive relationship with electrostatic induction.

As shown in Figure 5(d), the average diameters of the nanofibers remained unchanged with various feed rates from 10 to 30 mL/h when the air pressure was fixed at 0.2 MPa. However, the average diameters of nanofibers slightly increased from 144 to 150 nm for various feed rates from 10 to 30 mL/h when the air pressure was fixed at 0.1 MPa. No relevant interactive relationship existed between the air pressure and feed rate in the fitted model. As shown in Figure 5(e), the average diameters of nanofibers remained unchanged with various collection distances from 20 to 60 cm when the air pressure was fixed at 0.2 MPa. When the air pressure was as low as 0.1 MPa, the average diameters of the nanofibers increased from 145 to 159 nm with various collection distance from 20 to 60 cm. This result was attributed to the effect of the induction voltage. The electrostatic force was affected by the collection distance.[43] The induction voltage was more sufficient for spinning thinner fibers when the collection distance was closer. This observation revealed that the induction voltage had a strong interactive relationship with the collection distance.

Effect of the Feed Rate on the Fiber Morphology. The response surfaces of the average diameters of the nanofibers, in nanometers, as a function of the feed rate, are illustrated in Figure 5(b,d,f). At a low voltage such as 5 kV, the average diameters of nanofibers decreased slightly from 151 to 133 nm when the feed rate was increased from 10 to 30 mL/h. Obviously, the air pressure was the dominating drag force to spin thinner fibers. When the voltage was increased to 25 kV, the average diameters of nanofibers did not vary with the change in the feed rate because the drag force, which included the air pressure and electrostatic force, was sufficient.

Effect of the Collection Distance on the Fiber Morphology. The interactive relationship between the collection distance and induction voltage is shown in Figure 7.

The air pressure was the dominating drag force when the voltage was fixed at 5 kV. The average diameters of the nanofibers decreased slightly from 164 to 142 nm when the collection distance was increased from 20 to 60 cm. However, the fiber diameter increased from 110 to 144 nm when the collection distance was increased from 20 to 60 cm at a fixed voltage of 25 kV. Thus, the electrostatic force decreased with increasing collection distance. As stated earlier, a strong interaction existed between the collection distance and the induction voltage in the surface model.

CONCLUSIONS

In summary, EISBS was established by the introduction of an additional electrostatic field with an induction circle electrode into the SBS system. The process produced highly homogeneous and separated fibers. A response surface model based on the BBD model was constructed to investigate the relationship between the EISBS produced fiber diameters and the processing parameters. The results indicate that parameters, including the air pressure and induction voltage had significant effects on the average diameters of the nanofibers. An interactive effect

between the air pressure and induction voltage was also observed. Moreover, the fiber morphology, including the fiber diameter, separation, and dispersive properties, could be easily controlled by adjustment of the process variables.

ACKNOWLEDGMENTS

The authors acknowledge the National Natural Science Foundation of China (contract grant numbers 51103104 and 51473121), the Tianjin Natural Science Foundation (contract grant number 13JCZDJC32600), and the Technology Program of the Tianjin Municipal Education Commission (contract grant number 20130324) for their financial support.

REFERENCES

1. Benavides, R. E.; Jana, S. C.; Reneker, D. H. *ACS Macro Lett.* **2012**, *1*, 1032.
2. Pham, Q. P.; Sharma, U.; Mikos, A. G. *Tissue Eng.* **2006**, *12*, 1197.
3. Zhong, S. P.; Zhang, Y. Z.; Lim, C. T. *Wires Nanomed. Nanobiotechnol.* **2010**, *2*, 510.
4. Katti, D. S.; Robinson, K. W.; Ko, F. K. *J. Biomed. Mater. Res. B* **2004**, *70*, 286.
5. Mickova, A.; Buzgo, M.; Benada, O. *Biomacromolecules* **2012**, *13*, 952.
6. Yano, H.; Sugiyama, J.; Nakagaito, A. N. *Adv. Mater.* **2005**, *17*, 153.
7. Chang, J.; Dommer, M.; Chang, C. *Nano Energy* **2012**, *1*, 356.
8. Lou, H.; Li, W.; Li, C.; Wang, X. *J. Appl. Polym. Sci.* **2013**, *130*, 1383.
9. Hartgerink, J. D.; Beniash, E.; Stupp, S. I. *Science* **2001**, *294*, 1684.
10. Yan, X. B.; Han, Z. J.; Yang, Y.; Tay, B. K. *Sens. Actuators B* **2007**, *123*, 107.
11. Zhang, X.; Gou, W. J.; Manohar, S. K. *J. Am. Chem. Soc.* **2004**, *126*, 4502.
12. Li, W.; Wang, H. L. *J. Am. Chem. Soc.* **2004**, *126*, 2278.
13. Kim, S. H.; Nam, Y. S.; Lee, T. S. *Polym. J.* **2003**, *35*, 185.
14. Weitz, R. T.; Harnau, L.; Rauschenbach, S. *Nano Lett.* **2008**, *8*, 1187.
15. Zhuang, X.; Yang, X.; Shi, L.; Cheng, B.; Kang, W. *Carbohydr. Polym.* **2012**, *90*, 982.
16. Sinha-Ray, S.; Zhang, Y.; Yarin, A. L. *Biomacromolecules* **2011**, *12*, 2357.
17. Oliveira, J. E.; Moraes, E. A.; Costa, R. G. F. *J. Appl. Polym. Sci.* **2011**, *122*, 3396.
18. Zhuang, X.; Yang, X.; Shi, L. *Carbohydr. Polym.* **2012**, *90*, 982.
19. Oliveira, J. E.; Zucolotto, V.; Mattoso, L. H. C. *J. Nanosci. Nanotechnol.* **2012**, *12*, 2733.
20. Srinivasan, S.; Chhatre, S. S.; Mabry, J. M. *Polymer* **2011**, *52*, 3209.
21. Yan, G.; Zhuang, X.; Tao, X. *Sci. Adv. Mater.* **2013**, *5*, 209.
22. Abdal-Hay, A.; Barakat, N. A. M.; Lim, J. K. *Sci. Adv. Mater.* **2012**, *4*, 1268.
23. Sinha-Ray, S.; Yarin, A. L.; Pourdeyhimi, B. *Carbon* **2010**, *48*, 3575.
24. Zhuang, X.; Shi, L.; Jia, K. *J. Membr. Sci.* **2013**, *429*, 66.
25. Bianco, A.; Bozzo, B. M.; Del Gaudio, C.; Cacciotti, I.; Armentanno, I.; Dottori, M.; D'Angelo, F.; Martino, S.; Orlacchio, A.; Kenny, J. M. *J. Bioact. Compos. Polym.* **2011**, *26*, 225.
26. Rajendran, M.; Bhattacharya, A. K. *J. Eur. Ceram. Soc.* **2004**, *24*, 111.
27. Law, S. E. *J. Electrost.* **2001**, *51*, 25.
28. Walczak, Z. K. Processes of Fiber Formation; Elsevier Science: Oxford, **2002**; p 346.
29. Patel, M. K.; Ghanshyam, C.; Kapur, P. *J. Electrost.* **2013**, *71*, 55.
30. Wise, J. K.; Zussman, E.; Yarin, A. L.; Megaridis, C. M.; Cho, M. *Nanotechnol. Regen. Eng.* **2014**, 285.
31. Batz, N. G.; Mellors, J. S.; Alarie, J. P.; Ramsey, J. M. *Anal. Chem.* **2014**, *86*, 3493.
32. Khuri, A. I.; Mukhopadhyay, S. *Wires Comput. Stat.* **2010**, *2*, 128.
33. Guo, X.; Zou, X.; Sun, M. *Carbohydr. Polym.* **2010**, *80*, 344.
34. Shi, L.; Zhuang, X. P.; Tao, X.; Cheng, B.; Kang, W. *Fiber Polym.* **2013**, *14*, 1485.
35. Ferreira, S. L. C.; Bruns, R. E.; Ferreira, H. S.; Matosa, G. D.; Davida, J. M.; Brandãoa, G. C.; da Silvaa, E. G. P.; Portugala, L. A.; dos Reisc, P. S.; Souzaa, A. S.; dos Santosc, W. N. L. *Anal. Chim. Acta* **2007**, *597*, 179.
36. Ko, F. A. A.; Lam, H.; MacDiarmid, A. G. In Wearable Electronics and Photonics; Tao, X., Ed.; CRC: Cambridge: United Kingdom, **2005**; Chapter 2.
37. Regev, O.; Vandebril, S.; Zussman, E.; Clasen, C. *Polymer* **2010**, *51*, 2611.
38. Yu, J. H.; Fridrikh, S. V.; Rutledge, G. C. *Polymer* **2006**, *47*, 4789.
39. Vrbata, P.; Berka, P.; Stranska, D.; Dolezal, P.; Laznicek, M. *Int. J. Pharm.* **2014**, *437*, 407.
40. Kong, C. S.; Yoo, W. S.; Lee, K. Y. *J. Membr. Sci.* **2009**, *44*, 1107.
41. Um, I. C.; Fang, D. F.; Hsiao, B. S.; Okamoto, A.; Chu, B. *Biomacromolecules* **2004**, *5*, 1428.
42. Rabbi, A.; Nasouri, K.; Bahrambeygi, H.; Shoushtari, A. M.; Babaei, M. R. *Fiber Polym.* **2012**, *13*, 1007.
43. Wise, J. K.; Cho, M.; Zussman, E.; Megaridis, C. M.; Yarin, A. L. In Nanotechnology and Tissue Engineering. Laurencin, C. T.; Nair, L. S. Eds.; CRC Press, Taylor and Francis, **2008**; pp. 243–260.